GPS Solutions (2019) 23:56
https://doi.org/10.1007/s10291-019-0847-x

ORIGINAL ARTICLE

Performance of BDS-3: satellite visibility and dilution of precision

Minghua Wang[1,2] · Jiexian Wang[1] · Danan Dong[2] · Lingdong Meng[1,3] · Junping Chen[3] · Ahao Wang[1,3] · Haomeng Cui[1]

Received: 4 January 2019 / Accepted: 12 March 2019

Abstract
We describe a method to assess the performance of the third-generation BeiDou navigation satellite system (BDS-3), in terms of satellite visibility and dilution of precision (DOP), on global and regional scales. Different from traditional methods, this method estimates the satellite visibility and DOP without requiring real or simulated ephemerides. Validated by the reference values derived from real ephemerides of GPS and GLONASS, the estimated number of visible satellites achieves an accuracy better than 0.15, and the estimated DOP values are lower than their reference values by less than 10% on average. Applying this method to BDS-3, with a 5° cutoff elevation angle, results show that the geostationary earth orbit (GEO) and inclined geosynchronous orbit (IGSO) satellites of BDS-3 together contribute 3–6 visible satellites in the area of 60°S–60°N and 50°E–170°E. In this area, the number of visible BDS-3 satellites is 11–14, which is more than GPS and Galileo by 1–3, and GLONASS by 3–7. With better satellite visibility, the average BDS-3 horizontal, vertical, and time DOPs over this area are 0.74, 1.08, and 0.67, which are, respectively, 5%, 9%, and 3% lower than those of GPS and Galileo, 14%, 16%, and 21% lower than those of GLONASS, and 16%, 19% and 14% lower than those of the 24-MEO-only BDS-3.

Keywords BDS-3 · GNSS · Satellite observing probability · Satellite visibility · Dilution of precision

Introduction

Independently constructed by China, BeiDou navigation satellite system (BDS), as all global navigation satellite systems (GNSSs), is aiming to provide positioning, navigation, and timing (PNT) services for global users. The development of BDS is divided into three steps (CSNO 2019). With the successful deployment of two geostationary satellites, the BDS demonstration system (BDS-1) was formally established in late 2000, which determined user locations at the master control station (Bian et al. 2005). By the end of 2012, the second generation of BDS (BDS-2) was in full operation to provide regional services, which consists of five geostationary earth orbit (GEO) satellites, five inclined geosynchronous orbit (IGSO) satellites, and four medium earth orbit (MEO) satellites (Montenbruck et al. 2013; Yang et al. 2014). As the final step, a global system (BDS-3), consisting of 24 MEO, 3 GEO, and 3 IGSO satellites, is to be constructed, which is anticipated to provide world-wide services by 2020 (Yang 2010; Zhang et al. 2017).

The performance of BDS has been analyzed in many aspects, including signal carrier-to-noise density ratio (Hauschild et al. 2012; Xiao et al. 2016; Lou et al. 2018), precision of observations (Montenbruck et al. 2013; Yang et al. 2014), multipath effects (Wang et al. 2015; Wanninger et al. 2015; Cai et al. 2016), quality of broadcast ephemerides (Montenbruck and Steigenberger 2013; Zhang et al. 2016; Chen et al. 2017a), and BDS-2 wide-area differential correction system (Cao et al. 2012; Chen et al. 2017b). Although these investigations dealt with different aspects of BDS, all are related to its positioning accuracy. The GNSS positioning accuracy is not only determined by the ranging accuracy, but also by the geometry of constellations. Typically, variations in geometry on positioning accuracy are far greater than those in ranging accuracy for a certain constellation (Parkinson 1996). To relate the geometry of

✉ Jiexian Wang
wangjiexian@tongji.edu.cn

[1] College of Surveying and Geo-informatics, Tongji University, Shanghai 200092, China

[2] Engineering Center of SHMEC for Space Information and GNSS, East China Normal University, Shanghai 200241, China

[3] Shanghai Astronomical Observatory, Chinese Academy of Sciences, Shanghai 200030, China

Published online: 25 March 2019

constellations to positioning accuracy, dilution of precision (DOP) (Kihara and Okada 1984; Spilker 1996) is defined as a metric that acts as a mapping factor between the ranging error and positioning error. For BDS-2, the satellite visibility and DOP have been investigated on a global scale (Chiang et al. 2010; Yang et al. 2014) as well as specifically at the North Pole region (Yang and Xu 2016), and its contributions on improving the accuracy of multi-GNSS positioning have also been analyzed (Yang et al. 2011; Gumilar et al. 2018).

Since BDS-3 is still under construction, it has not been studied thoroughly as the completed BDS-2, though some initial results based on few early deployed BDS-3 satellites are provided in Zhang et al. (2017, 2018). As BDS-3 entered into an intense launch period in 2018 (19 BDS-3 satellites had been launched from November 2017 to November 2018), we are at the very time of the transition of BDS-2 to BDS-3. In this context, as a step toward gaining more knowledge of BDS-3 performance, we aim to estimate the satellite visibility and DOP of the forthcoming full BDS-3 constellation. Most calculations of satellite visibility and DOP are based on actual (Yahya and Kamarudin 2008; Yang et al. 2014) or simulated (Meng et al. 2004; Eissfeller et al. 2007; Chiang et al. 2010) ephemerides. However, the actual ephemerides for the full constellation are not available before all satellites are deployed, and the results based on simulated almanacs are highly dependent on the accuracy of the simulations. Wang et al. (2002) presented a method that estimates the satellite visibility and DOP just with a few orbit parameters, and this method was later used by Chen (2007) to calculate the GNSS DOP at low earth orbit (LEO) satellites. By revisiting their method, we find that the satellite observing probability, the foundation of the method, was defined without taking into account some potential conditions, which increases the discrepancy between the estimates and the observed results. Moreover, the method is only for MEO constellations. We present a modified definition of the satellite observing probability that gives better estimation results, and we extend the method to be applicable to the hybrid constellation of BDS-3. To validate the modified definition and the estimating method, we compare the estimated satellite visibility and DOP with reference values derived from real precise ephemerides of GPS and GLONASS. Then we estimate and analyze the global and regional satellite visibility and DOP of BDS-3, both the 24-MEO-only and full-constellation BDS-3, and also of GPS, GLONASS, and Galileo for comparisons.

Methodology

The orbit of a GNSS satellite is approximately a circle. Satellites at different orbits with a same radius run along the surface of the sphere with that radius, hereinafter referred to as spherical orbit surface. The probability of satellites to be observed within divided blocks on their spherical orbit surface, referred to as satellite observing probability, is the basis for the estimation of satellite visibility and DOP. We present a modified definition of satellite observing probability for GNSS MEO satellites and the definitions of BDS-3 GEO and IGSO satellite observing probabilities. Based on these definitions we then introduce the method for estimating satellite visibility and DOP.

GNSS parameters

Table 1 shows the values of constellation parameters involved in the calculation of satellite observing probability. Recent precise ephemerides show that there are 29–32, on average 31, available GPS satellites on individual days. For BDS-3, GLONASS, and Galileo, the number of available satellites is less than the nominal number. Thus, to assess the full-constellation performance, we use the nominal number for BDS-3, GLONASS, and Galileo, and use 31 for GPS in probability calculations.

MEO satellite observing probability

In earth centered earth fixed (ECEF) system, when a GNSS MEO satellite is at a position with geocentric latitude φ and longitude λ on the spherical orbit surface, its angular velocity in the north–south direction ω_{NS} and in the east–west direction ω_{EW} are (Wang et al. 2002; Chen 2007)

$$\begin{cases} \omega_{\mathrm{NS}} = \omega\sqrt{1-\left(\frac{\cos i_{\mathrm{orb}}}{\cos\varphi}\right)^2} \\ \omega_{\mathrm{EW}} = \frac{\omega\cos i_{\mathrm{orb}}}{\cos^2\varphi} - \omega_{\mathrm{Earth}} \end{cases} \tag{1}$$

where ω is the satellite angular velocity in the orbital plane. ω_{Earth} is the angular velocity of the earth. i_{orb} is the orbit inclination.

Table 1 Parameter nominal values of BDS-3, GPS, GLONASS, and Galileo (Hofmann-Wellenhof et al. 2007; Yang et al. 2017; CSNO 2019)

Parameter	BDS-3			GPS	GLONASS	Galileo
Orbit type	MEO	IGSO	GEO	MEO	MEO	MEO
Nominal number	24	3	3	24 (31)	24	30
Inclination	55°	55°	0°	55°	64.8°	56°
Altitude (km)	21,528	35,786	35,786	20,200	19,100	23,222
Period (s)	46,404	86,164	86,164	43,080	40,544	50,685

Wang et al. (2002) divided the spherical orbit surface into areas with equally angular spacing in both north–south and east–west directions. They thought that the opportunities of a satellite to be observed in the areas were inversely proportional to its angular velocities, and defined the satellite observing probability as

$$P^{\mathrm{M}}(\varphi)=\begin{cases}\frac{k}{\sqrt{\omega_{\mathrm{NS}}^2+\omega_{\mathrm{EW}}^2}} & |\varphi|<i_{\mathrm{orb}}\\ 0 & |\varphi|\geq i_{\mathrm{orb}}\end{cases} \tag{2}$$

where k is a constant for a certain GNSS. The superscript M means that the probability is for MEO satellites.

For a certain GNSS, because i_{orb} and ω of MEO satellites are assumed to be constant, satellites at a same geocentric latitude φ have equal ω_{NS} and ω_{EW} velocities (1). However, Wang et al. (2002) neglected this fact when they defined the satellite observing probability. Imaging that satellites travel from an arbitrary 1°×1° grid cell centered on (φ_0, λ_0) to its east adjacent cell, whereas some other satellites fly from its west adjacent grid cell to this cell with the same east–west angular velocity. Based on the assumption of symmetrical satellite distribution in the east–west direction (Wang et al. 2002), the in and out satellites of the grid cell centered on (φ_0, λ_0) are balanced in this direction. This indicates that the observing probability is independent of the satellite east–west angular velocity. Nevertheless, in the north–south direction, the in and out satellites of the grid cell cannot be balanced due to unequal satellite angular velocity at adjacent cells in this direction. Thus, the satellite observing probability depends on the north–south angular velocity, and we modify the definition as

$$P^{\mathrm{M}}(\varphi)=\begin{cases}\frac{k}{\omega_{\mathrm{NS}}}=\frac{k\cos\varphi}{\omega\sqrt{\cos^2\varphi-\cos^2 i_{\mathrm{orb}}}} & |\varphi|<i_{\mathrm{orb}}\\ 0 & |\varphi|\geq i_{\mathrm{orb}}\end{cases} \tag{3}$$

For comparison, Eqs. (2) and (3) are referred to as the original definition and the modified definition, respectively.

If the spherical orbit surface is divided into 1°×1° grid cells centered on (φ_i, λ_j)

$$\begin{cases}\varphi_i=i-0.5 & i=-89,-88,...,90\\ \lambda_j=j-0.5 & j=1,2,...,360\end{cases} \tag{4}$$

then for an n-satellite GNSS, the summation of the satellite observing probabilities over all grid cells satisfies

$$\sum_{i=-89}^{90}\sum_{j=1}^{360}P_{ij}^{\mathrm{M}}=n \tag{5}$$

where P_{ij}^{M} is the satellite observing probability of grid cell centered on(φ_i, λ_j).

Using Eq. (5), the constant k in (3) can be determined. By determining the constant k for each GNSS, we calculated the latitudinal distribution of satellite observing probability on the spherical orbit surface for each system (Fig. 1). The satellite observing probability of the 24-MEO-only BDS-3 (M-BDS-3) is less than that of GPS and Galileo because there are less satellites in its constellation. However, its satellite observing probability is greater than that of the 24-satellite GLONASS. This is because GLONASS has a larger orbit inclination and its satellites cover a wider range of latitudes, which disperses the probability latitudinal distribution.

BDS-3 GEO and IGSO satellite observing probability

The 3 BDS-3 GEO satellites are located at 80°E, 110.5°E, and 140°E (CSNO 2019) (Fig. 2). For the 3 IGSO satellites, the ground tracks are coincident while the longitude of the intersection point is at 118°E, with a phase difference of 120° (CSNO 2012).

In the ECEF system, GEO satellites are stationary, thus, their observing probability at an arbitrary position (φ, λ) on the spherical orbit surface is

$$P^{\mathrm{G}}(\varphi,\lambda)=\begin{cases}1 & (\varphi,\lambda)\in\Lambda\\ 0 & \text{other positions}\end{cases} \tag{6}$$

where Λ is the set of GEO satellite positions, which are (0, 80°), (0, 110.5°), and (0, 140°) for BDS-3. The superscript G means that the probability is for GEO satellites.

An IGSO satellite runs along a figure-8-shape path on the spherical orbit surface in the ECEF system. The probability

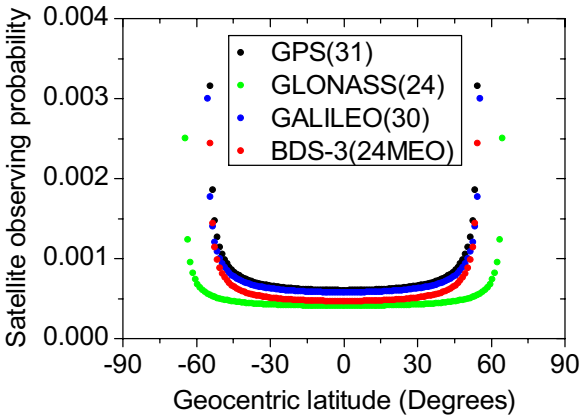

Fig. 1 Latitudinal distributions of satellite observing probability on the spherical orbit surface for M-BDS-3, GPS (31-satellite), GLONASS (24-satellite), and Galileo (30-satellite). Each value is a satellite observing probability for a 1°×1° grid cell and the corresponding horizontal coordinate is the central latitude of the cell

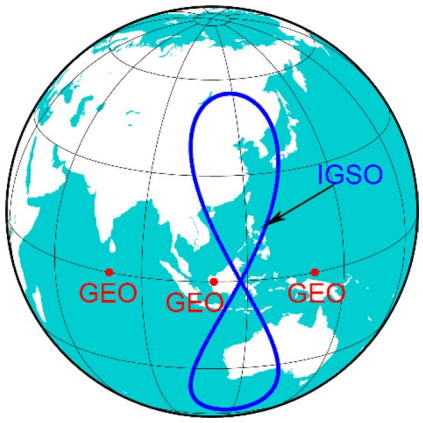

Fig. 2 Nominal ground tracks of BDS-3 GEO and IGSO satellites

of an IGSO satellite to be observed within a grid cell is inversely proportional to its stay duration, and that duration depends on the larger of the east–west and north–south satellite angular velocities. Thus, we define the IGSO satellite observing probability as

$$P^{\mathrm{I}}(\varphi)=\begin{cases}\dfrac{k'}{\max[\omega_{\mathrm{EW}}(\varphi),\omega_{\mathrm{NS}}(\varphi)]} & (\varphi,\lambda)\in\Gamma\\ 0 & (\varphi,\lambda)\notin\Gamma\end{cases} \tag{7}$$

where k' is a constant. Γ is the figure-8-shape orbit. $\max[\omega_{\mathrm{EW}}(\varphi),\omega_{\mathrm{NS}}(\varphi)]$ is the larger of $\omega_{\mathrm{EW}}(\varphi)$ and $\omega_{\mathrm{NS}}(\varphi)$. The superscript I means that the probability is for IGSO satellites.

Considering both the accuracy and computation, we used 0.5°×0.5° grid cells to calculate the IGSO satellite observing probability. The grid cell centers are (φ_i,λ_j).

$$\begin{cases}\varphi_i=0.5i-0.25 & i=-179,-178,...,180\\ \lambda_j=0.5j-0.25 & j=1,2,...,720\end{cases} \tag{8}$$

We retrieved all the $0.5^\circ\times0.5^\circ$ grid cells along the figure-8-shape orbit of BDS-3 IGSO satellites (see Appendix 1 for details), and named the set of these cells Ψ. The satellite observing probabilities of all grid cells for n IGSO satellites satisfy

$$\sum_{i=-179}^{180}\sum_{j=1}^{720}P_{ij}^{\mathrm{I}}=\sum_{(\varphi_i,\lambda_j)\in\Psi}\frac{k'}{\max[\omega_{\mathrm{EW}}(\varphi_i),\omega_{\mathrm{NS}}(\varphi_i)]}=n \tag{9}$$

where P_{ij}^{I} is the satellite observing probability of grid cell centered on (φ_i,λ_j). Using Eq. (9), the constant k' can be determined.

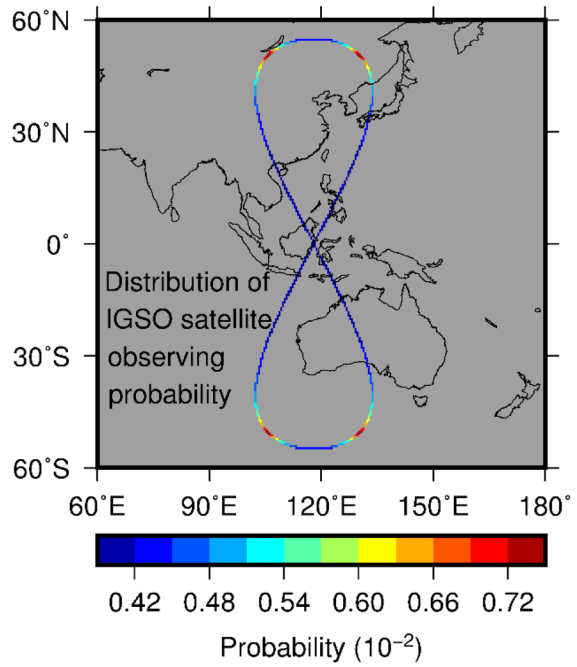

Fig. 3 Distribution of BDS-3 IGSO satellite observing probability

We calculated the satellite observing probability of the 3 BDS-3 IGSO satellites for each grid cell (Fig. 3). The probability distribution shows that the values are larger at the grid cells near the north and south ends of the figure-8-shape track.

Estimation of satellite visibility and DOP

For a GNSS of MEO-satellite constellation, the number of visible satellites above a cutoff elevation angle (CEA) over a station can be estimated as

$$n_{\mathrm{vis}}=\sum_{E_{ij}>E_0}P_{ij}^{\mathrm{M}} \tag{10}$$

While for the full-constellation BDS-3, the satellite visibility is estimated as

$$n_{\mathrm{vis}}=\sum_{E_{ij}>E_0}P_{ij}^{\mathrm{M}}+\sum_{\substack{(\varphi_i,\lambda_j)\in\Lambda\\ E_{ij}>E_0}}P_{ij}^{\mathrm{G}}+\sum_{\substack{(\varphi_i,\lambda_j)\in\Psi\\ E_{ij}>E_0}}P_{ij}^{\mathrm{I}} \tag{11}$$

where E_{ij} is the elevation angle of the grid cell centered on (φ_i,λ_j). E_0 is the CEA.

Assuming that n satellites are observed at an epoch, the coefficient matrix of the linearized observation equations is (Hofmann-Wellenhof et al. 2007)

$$A=\begin{pmatrix} e_{x1} & e_{y1} & e_{z1} & -1 \\ e_{x2} & e_{y2} & e_{z2} & -1 \\ \vdots & \vdots & \vdots & \vdots \\ e_{xn} & e_{yn} & e_{zn} & -1 \end{pmatrix} \tag{12}$$

where $\begin{pmatrix} e_{xi} & e_{yi} & e_{zi} \end{pmatrix}^{\mathrm{T}}$ is the i-th satellite-to-station unit vector. Then the coefficient matrix of the normal equation is

$$N_{aa}=A^{\mathrm{T}}A=\begin{pmatrix} \sum_{i=1}^{n} e_{xi}^2 & \sum_{i=1}^{n} e_{xi}e_{yi} & \sum_{i=1}^{n} e_{xi}e_{zi} & -\sum_{i=1}^{n} e_{xi} \\ \sum_{i=1}^{n} e_{yi}e_{xi} & \sum_{i=1}^{n} e_{yi}^2 & \sum_{i=1}^{n} e_{yi}e_{zi} & -\sum_{i=1}^{n} e_{yi} \\ \sum_{i=1}^{n} e_{zi}e_{xi} & \sum_{i=1}^{n} e_{zi}e_{yi} & \sum_{i=1}^{n} e_{zi}^2 & -\sum_{i=1}^{n} e_{zi} \\ -\sum_{i=1}^{n} e_{xi} & -\sum_{i=1}^{n} e_{yi} & -\sum_{i=1}^{n} e_{zi} & n \end{pmatrix} \tag{13}$$

and the cofactor matrix is

$$Q=N_{aa}^{-1} \tag{14}$$

By definition, the DOPs can be calculated as

$$\begin{cases} \mathrm{NDOP}=\sqrt{Q_{\mathrm{NEUT}}(1,1)}\ \text{North DOP} \\ \mathrm{EDOP}=\sqrt{Q_{\mathrm{NEUT}}(2,2)}\ \text{East DOP} \\ \mathrm{VDOP}=\sqrt{Q_{\mathrm{NEUT}}(3,3)}\ \text{Vertical DOP} \\ \mathrm{TDOP}=\sqrt{Q_{\mathrm{NEUT}}(4,4)}\ \text{Time DOP} \\ \mathrm{HDOP}=\sqrt{\mathrm{NDOP}^2+\mathrm{EDOP}^2}\ \text{Horizontal DOP} \\ \mathrm{PDOP}=\sqrt{\mathrm{HDOP}^2+\mathrm{VDOP}^2}\ \text{Position DOP} \\ \mathrm{GDOP}=\sqrt{\mathrm{PDOP}^2+\mathrm{TDOP}^2}\ \text{Geometry DOP} \end{cases} \tag{15}$$

where Q_{NEUT} represents the cofactor matrix expressed in topocentric coordinate system.

In our case, the exact number and positions of the satellites in view are unknown, hence it is not straightforward to get A and N_{aa}. We established an observation equation for each grid cell with elevation angle greater than the CEA, and used satellite observing probabilities of the grid cells as their weights. Then the A and N_{aa} can be obtained. The coefficient matrix of the normal equations for BDS-3 is

$$N_{aa}^{\mathrm{MGI}}=N_{aa}^{\mathrm{M}}+N_{aa}^{\mathrm{G}}+N_{aa}^{\mathrm{I}} \tag{16}$$

where

$$N_{aa}^{\mathrm{M}}=\begin{pmatrix} \sum_{i=-89}^{90}\sum_{j=1}^{360} P_{ij}^{\mathrm{M}}e_{xij}^2 & \sum_{i=-89}^{90}\sum_{j=1}^{360} P_{ij}^{\mathrm{M}}e_{xij}e_{yij} & \sum_{i=-89}^{90}\sum_{j=1}^{360} P_{ij}^{\mathrm{M}}e_{xij}e_{zij} & -\sum_{i=-89}^{90}\sum_{j=1}^{360} P_{ij}^{\mathrm{M}}e_{xij} \\ \sum_{i=-89}^{90}\sum_{j=1}^{360} P_{ij}^{\mathrm{M}}e_{yij}e_{xij} & \sum_{i=-89}^{90}\sum_{j=1}^{360} P_{ij}^{\mathrm{M}}e_{yij}^2 & \sum_{i=-89}^{90}\sum_{j=1}^{360} P_{ij}^{\mathrm{M}}e_{yij}e_{zij} & -\sum_{i=-89}^{90}\sum_{j=1}^{360} P_{ij}^{\mathrm{M}}e_{yij} \\ \sum_{i=-89}^{90}\sum_{j=1}^{360} P_{ij}^{\mathrm{M}}e_{zij}e_{xij} & \sum_{i=-89}^{90}\sum_{j=1}^{360} P_{ij}^{\mathrm{M}}e_{zij}e_{yij} & \sum_{i=-89}^{90}\sum_{j=1}^{360} P_{ij}^{\mathrm{M}}e_{zij}^2 & -\sum_{i=-89}^{90}\sum_{j=1}^{360} P_{ij}^{\mathrm{M}}e_{zij} \\ -\sum_{i=-89}^{90}\sum_{j=1}^{360} P_{ij}^{\mathrm{M}}e_{xij} & -\sum_{i=-89}^{90}\sum_{j=1}^{360} P_{ij}^{\mathrm{M}}e_{yij} & -\sum_{i=-89}^{90}\sum_{j=1}^{360} P_{ij}^{\mathrm{M}}e_{zij} & \sum_{i=-89}^{90}\sum_{j=1}^{360} P_{ij}^{\mathrm{M}} \end{pmatrix}_{E_{ij}>E_0} \tag{17}$$

$$N_{aa}^{\mathrm{G}}=\begin{pmatrix} \sum_{(\varphi_i,\lambda_j)\in\Lambda} P_{ij}^{\mathrm{G}}e_{xij}^2 & \sum_{(\varphi_i,\lambda_j)\in\Lambda} P_{ij}^{\mathrm{G}}e_{xij}e_{yij} & \sum_{(\varphi_i,\lambda_j)\in\Lambda} P_{ij}^{\mathrm{G}}e_{xij}e_{zij} & -\sum_{(\varphi_i,\lambda_j)\in\Lambda} P_{ij}^{\mathrm{G}}e_{xij} \\ \sum_{(\varphi_i,\lambda_j)\in\Lambda} P_{ij}^{\mathrm{G}}e_{yij}e_{xij} & \sum_{(\varphi_i,\lambda_j)\in\Lambda} P_{ij}^{\mathrm{G}}e_{yij}^2 & \sum_{(\varphi_i,\lambda_j)\in\Lambda} P_{ij}^{\mathrm{G}}e_{yij}e_{zij} & -\sum_{(\varphi_i,\lambda_j)\in\Lambda} P_{ij}^{\mathrm{G}}e_{yij} \\ \sum_{(\varphi_i,\lambda_j)\in\Lambda} P_{ij}^{\mathrm{G}}e_{zij}e_{xij} & \sum_{(\varphi_i,\lambda_j)\in\Lambda} P_{ij}^{\mathrm{G}}e_{zij}e_{yij} & \sum_{(\varphi_i,\lambda_j)\in\Lambda} P_{ij}^{\mathrm{G}}e_{zij}^2 & -\sum_{(\varphi_i,\lambda_j)\in\Lambda} P_{ij}^{\mathrm{G}}e_{zij} \\ -\sum_{(\varphi_i,\lambda_j)\in\Lambda} P_{ij}^{\mathrm{G}}e_{xij} & -\sum_{(\varphi_i,\lambda_j)\in\Lambda} P_{ij}^{\mathrm{G}}e_{yij} & -\sum_{(\varphi_i,\lambda_j)\in\Lambda} P_{ij}^{\mathrm{G}}e_{zij} & \sum_{(\varphi_i,\lambda_j)\in\Lambda} P_{ij}^{\mathrm{G}} \end{pmatrix}_{E_{ij}>E_0} \tag{18}$$

$$N_{aa}^{\mathrm{I}}=\begin{pmatrix} \sum_{(\varphi_i,\lambda_j)\in\Psi} P_{ij}^{\mathrm{I}}e_{xij}^2 & \sum_{(\varphi_i,\lambda_j)\in\Psi} P_{ij}^{\mathrm{I}}e_{xij}e_{yij} & \sum_{(\varphi_i,\lambda_j)\in\Psi} P_{ij}^{\mathrm{I}}e_{xij}e_{zij} & -\sum_{(\varphi_i,\lambda_j)\in\Psi} P_{ij}^{\mathrm{I}}e_{xij} \\ \sum_{(\varphi_i,\lambda_j)\in\Psi} P_{ij}^{\mathrm{I}}e_{yij}e_{xij} & \sum_{(\varphi_i,\lambda_j)\in\Psi} P_{ij}^{\mathrm{I}}e_{yij}^2 & \sum_{(\varphi_i,\lambda_j)\in\Psi} P_{ij}^{\mathrm{I}}e_{yij}e_{zij} & -\sum_{(\varphi_i,\lambda_j)\in\Psi} P_{ij}^{\mathrm{I}}e_{yij} \\ \sum_{(\varphi_i,\lambda_j)\in\Psi} P_{ij}^{\mathrm{I}}e_{zij}e_{xij} & \sum_{(\varphi_i,\lambda_j)\in\Psi} P_{ij}^{\mathrm{I}}e_{zij}e_{yij} & \sum_{(\varphi_i,\lambda_j)\in\Psi} P_{ij}^{\mathrm{I}}e_{zij}^2 & -\sum_{(\varphi_i,\lambda_j)\in\Psi} P_{ij}^{\mathrm{I}}e_{zij} \\ -\sum_{(\varphi_i,\lambda_j)\in\Psi} P_{ij}^{\mathrm{I}}e_{xij} & -\sum_{(\varphi_i,\lambda_j)\in\Psi} P_{ij}^{\mathrm{I}}e_{yij} & -\sum_{(\varphi_i,\lambda_j)\in\Psi} P_{ij}^{\mathrm{I}}e_{zij} & \sum_{(\varphi_i,\lambda_j)\in\Psi} P_{ij}^{\mathrm{I}} \end{pmatrix}_{E_{ij}>E_0} \tag{19}$$

where $(e_{xij}\ e_{yij}\ e_{zij})^{\mathrm{T}}$ is the unit vector of the grid cell centered on (φ_i, λ_j) to the station. For the full constellation BDS-3, N_{aa}^{MGI} is used to estimate the DOP, while for M-BDS-3 or other MEO-constellation GNSSs, N_{aa}^{M} is used.

Method validation

To validate the modified definition of satellite observing probability and assess the method of satellite visibility and DOP estimation, we used 24-h averages of the values derived from GPS and GLONASS precise ephemerides as the references. There are 21–23 available GLONASS satellites on individual days, and we failed to calculate the GLONASS DOP at some latitudes and epochs due to lack of minimal number of visible satellites. Thus, GLONASS is only used to validate satellite visibility estimation.

Figure 4 shows the estimates of the number of visible satellites and their corresponding reference values at different latitudes for different CEAs. For both GPS and GLONASS, the number estimated with the modified satellite observing probability agrees better with its reference value than that with original defined one. Using the modified probability, the root mean squares (RMSs) between the estimated and reference number of visible satellites are on average 0.13 for GPS and 0.02 for GLONASS.

Figure 5 shows the estimated and reference GPS DOPs for 5° and 10° CEAs. The estimated DOPs are less than their reference values, but they reflect well the variations of the references over different latitudes. In general, the discrepancies between estimated and reference values at middle latitudes are larger than at other locations. As the CEA increases, both the DOP values and the discrepancies between the estimated and reference values increase as well.

To quantify the DOP underestimation, the underestimating rates for different GPS constellations, i.e., constellations with different number of satellites, are calculated (Table 2). With a 5° CEA, the average underestimating rates are 7–11% for the DOPs. As the CEA increases to 10°, the average underestimating rates are increased by 1–2% for each kind of DOP (not shown). Thus, to ensure a higher accuracy, we apply the 5° CEA for the following DOP calculations.

Results

Within this section, the satellite visibility and DOP of M-BDS-3 and BDS-3 are estimated and compared with those of GPS, GLONASS, and Galileo. For BDS-3, to analyze the contribution of GEO and IGSO satellites, we placed the emphasis on an area located in the Asia-Pacific region.

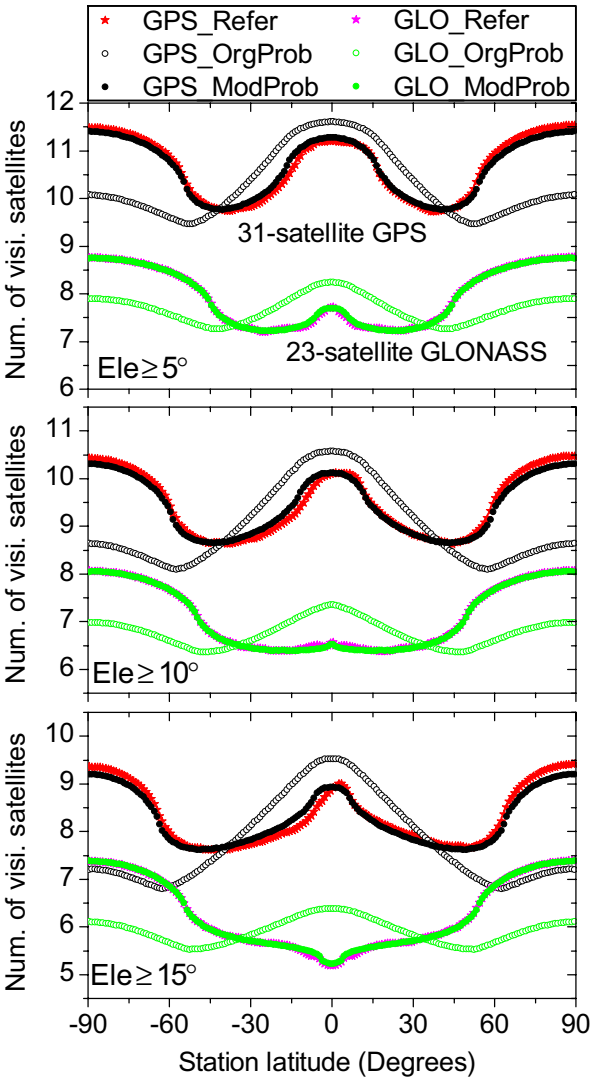

Fig. 4 Estimated and reference numbers of visible satellites of 31-satellite GPS and 23-satellite GLONASS at all latitudes for the CEA of 5°, 10°, and 15°. The numbers are estimated, respectively, with the modified (the solid circles) and original (the hollow circles) satellite observing probabilities. The reference values (the stars) are derived from precise ephemerides. See legend on the top of the figure

Performance of M-BDS-3

The estimates show that with a 5° CEA, 8–9 satellites of M-BDS-3 can be observed for all latitudes (Fig. 6). Less M-BDS-3 satellites tend to be observed over middle latitudes (30°–60°) than other latitudes. GPS and Galileo have similar latitudinal distributions of the number of visible satellites as M-BDS-3, but they have about two more satellites in view than M-BDS-3 at any latitude. Below 37° latitude, more satellites of M-BDS-3 than GLONASS are likely to be observed, while at the latitudes greater than 37°, the opposite is the case. For each GNSS, as the CEA increases, the number of visible satellites reduces, while its latitudinal distribution is similar.

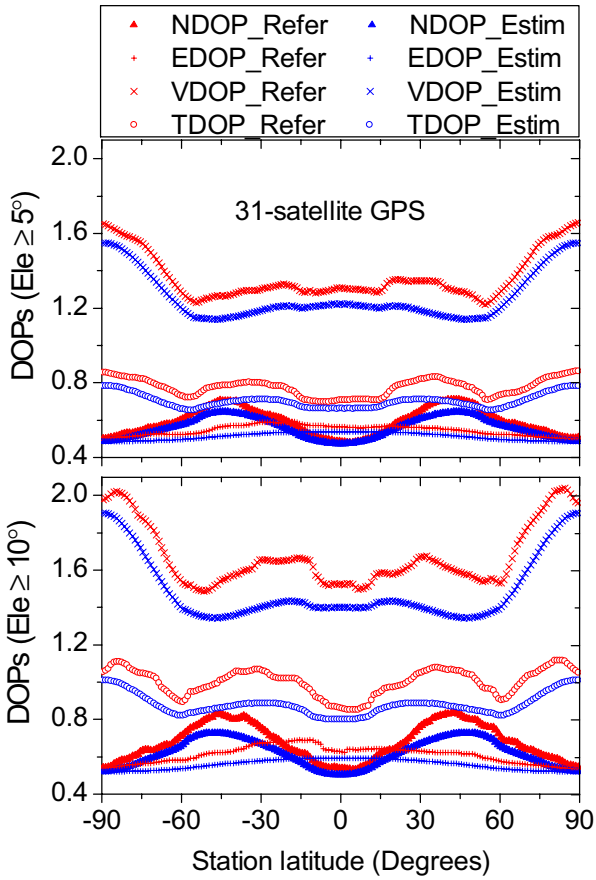

Fig. 5 Estimated (blue) and reference (red) DOPs of the 31-satellite GPS at all latitudes. See legend on the top of the figure

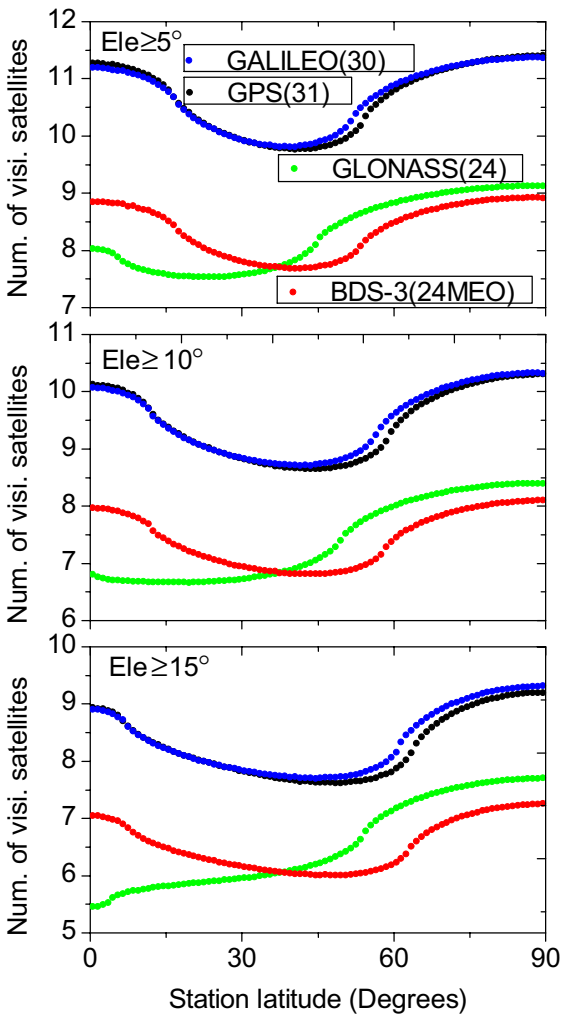

Fig. 6 Estimated number of visible satellites of M-BDS-3, GPS, GLONASS, and Galileo at different latitudes for 5°, 10°, and 15° CEAs. The legends of the middle and bottom panels are the same as in the top panel

Table 2 Average, minimal, and maximal underestimating rates of the estimated GPS DOPs relative to the reference values ($\frac{\text{refer.}-\text{estm.}}{\text{refer.}} \times 100\%$) over the latitudes

Num. of Sat.	Underestimating rates of GPS DOPs (%) Ave. (Min.~Max.)			
	HDOP	VDOP	PDOP	TDOP
32	7 (4 ~ 11)	8 (3 ~ 13)	8 (5 ~ 13)	9 (3 ~ 16)
31	7 (5 ~ 12)	8 (3 ~ 13)	8 (4 ~ 12)	10 (2 ~ 18)
30	7 (3 ~ 15)	8 (4 ~ 15)	8 (4 ~ 16)	10 (3 ~ 22)
29	7 (3 ~ 14)	8 (3 ~ 16)	8 (4 ~ 18)	11 (3 ~ 21)

The underestimating rates are calculated for 29-satellite, 30-satellite, 31-satellite, and 32-satellite GPS with a 5° CEA

In general, the estimated DOPs of M-BDS-3 have similar latitudinal distributions as those of GPS and Galileo, but with greater values (Fig. 7). For each GNSS, the EDOP decreases slowly from the equator to the pole (panel a), and a crest (maximal value) of the NDOP occurs around the latitude of 40° (panel b). The NDOP-to-EDOP ratios are less than 1 near the equator and close to 1 near the pole (panel f). At the pole, the HDOP reaches its minimum (panel c), while the VDOP has its maximum (panel d), except for GLONASS, whose maximal VDOP occurs around 18° latitude.

Figure 7 (panel f) shows that the NDOP-to-EDOP ratios of 55°-orbit-inclination M-BDS-3 and GPS are larger than that of 56°-orbit-inclination Galileo, and the latter is in turn larger than that of 64.8°-orbit-inclination GLONASS. This indicates that the constellation design of a higher orbit inclination improves the north accuracy compared to the east accuracy.

Performance of BDS-3

Globally, the region of one or more visible BDS-3 GEO satellites covers a wider range in the east–west direction than

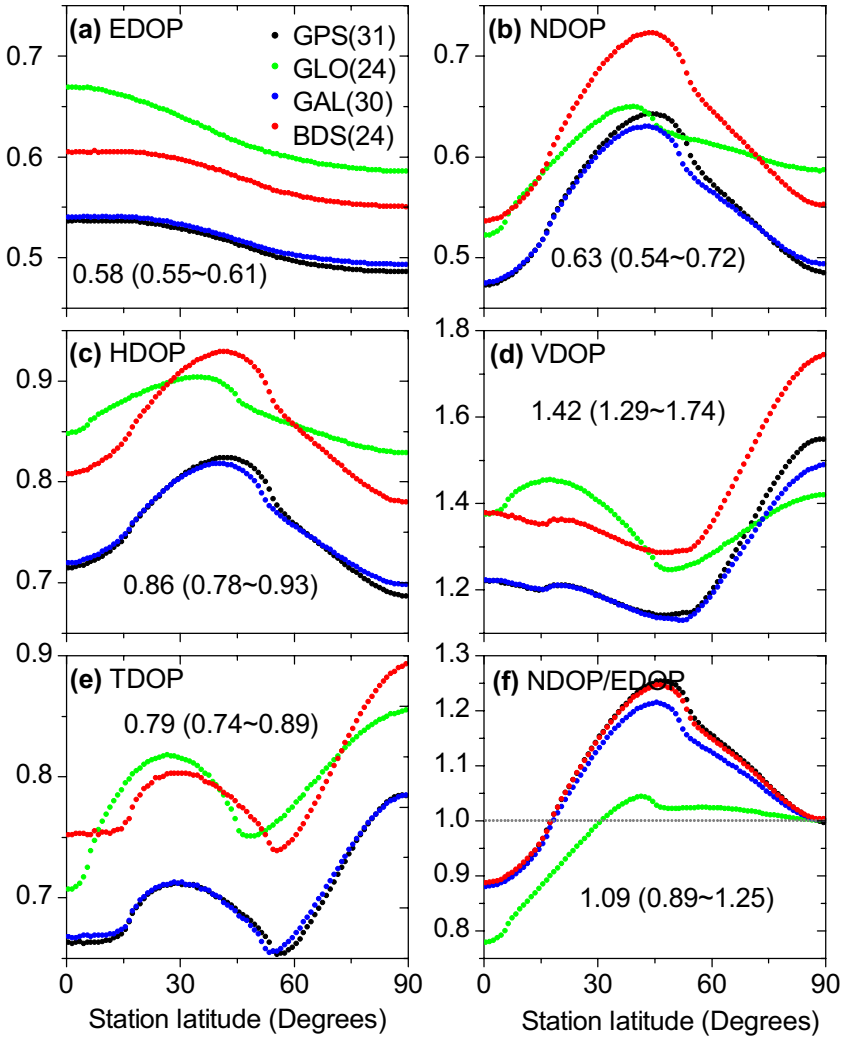

Fig. 7 Estimated DOPs of M-BDS-3 and the other three GNSSs at different latitudes with a 5° CEA. **a** east DOP; **b** north DOP; **c** horizontal DOP; **d** vertical DOP; **e** time DOP; **f** NDOP-to-EDOP ratio. The numerical values marked in each subplot are the average, minimal, maximal DOPs of M-BDS-3 over the latitudes. The legends of **b**–**f** are the same as in **a**

that of IGSO satellites, while the latter covers a wider range in the north–south direction (Fig. 8 top and middle). Over about two-thirds of the global areas, the satellite visibilities are improved with varying degrees due to the enhancement of the 3 GEO and 3 IGSO satellites (Fig. 8 bottom). In the study area of 60°S–60°N and 50°E–170°E, the number of visible satellites of BDS-3 is more than M-BDS-3 by 3–6, and the most improved area is located in the center, including Southeast Asia and Northwestern Australia.

The estimated number of BDS-3 visible satellites over the global locations is about 8–14 (Fig. 9). In the study area, 11 or more BDS-3 satellites can be observed. The average number of visible satellites in this area reaches 13.2, more than the global average by 2.7.

In this study area, the number of visible BDS-3 satellites is 1–3 more than GPS and Galileo, and 3–7 more than GLONASS (Fig. 10). Particularly, in the areas of Australia and most parts of Asia, there are 3 more visible satellites of BDS-3 than GPS and Galileo, and 5 more visible satellites of BDS-3 than GLONASS.

Figure 11 shows the estimated DOPs of BDS-3 in the study area. The EDOP generally decreases from the central longitude of the area to the east and west end, while the NDOP basically increases from the equator to middle latitudes. Ranging from 0.66 to 0.80 (average: 0.74), the HDOP is smaller at 0°–15° latitudes and the north and south ends than at 30°–50° latitudes. The VDOP, ranging from 0.98 to 1.21 (average: 1.08), is less than 1 in Southeast Asia and Northern Australia. The TDOP is from 0.56 to 0.75 (average: 0.67), and the PDOP and GDOP (not shown) range from 1.19 to 1.44 (average: 1.30) and 1.32 to 1.61 (average: 1.47), respectively. From the center of the area to the periphery, the NDOP-to-EDOP ratio, ranging from 0.86 to 1.30 (average: 1.05), becomes larger. In the areas enclosed by the contours of the NDOP-to-EDOP ratios equal to 1 (blue), the east positioning accuracy is higher than the north, while in other areas (red), the opposite is the case.

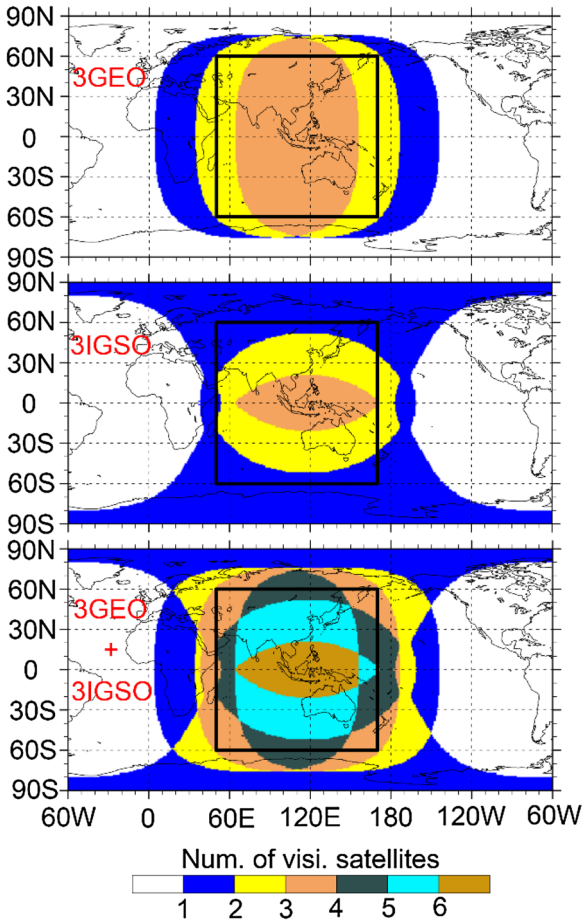

Fig. 8 Estimated number of visible BDS-3 GEO (top), IGSO (middle), and GEO + IGSO (bottom) satellites with a 5° CEA. The black squares enclose the study area

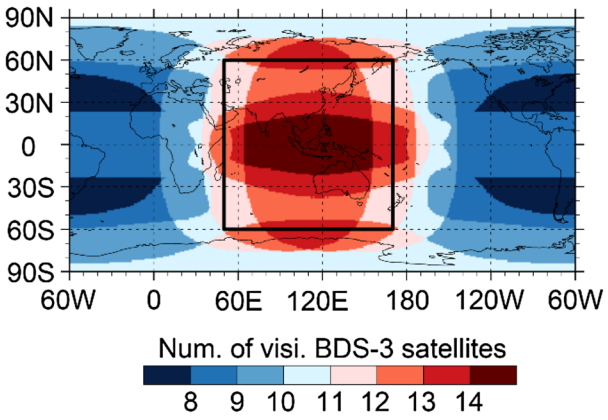

Fig. 9 Estimated number of BDS-3 visible satellites with a 5° CEA. The study area is enclosed by the black square

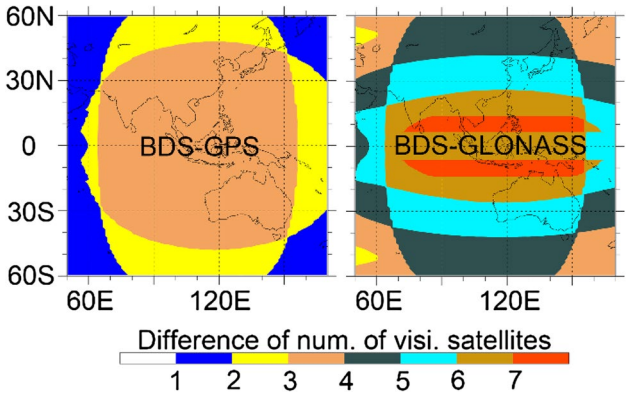

Fig. 10 Differences of the number of visible satellites between BDS-3 and the 31-satellite GPS (left) and between BDS-3 and the 24-satellite GLONASS (right). The differences are number of BDS-3 visible satellites minus those of the other GNSSs. Because the differences between BDS-3 and the 30-satellite Galileo are similar to those between BDS-3 and GPS, they are not shown in the figure

The DOPs derived from BDS-3 GEO + MEO, IGSO + MEO, and full constellation (GEO + IGSO + MEO) are compared with those from M-BDS-3 (MEO only) to investigate the impact of GEO and IGSO satellites on DOP improvements (Table 3). Adding the 3 GEO satellites to M-BDS-3 on average reduces the HDOP, VDOP, PDOP, and TDOP in the study area by 10%, 11%, 11%, and 8%, respectively. The 3 IGSO satellites bring similar average DOP improvements as the GEO satellites, but the DOP improving rates are concentrated in smaller ranges. When both the GEO and IGSO satellites are added, the average improving rates reach 16% for HDOP, 19% for VDOP, 18% for PDOP, and 14% for TDOP.

Over the study area, the average DOPs of BDS-3 are less than those of the other three GNSSs (Table 4). Compared with GPS and Galileo, the averages of BDS-3 HDOP, VDOP, PDOP, and TDOP are, respectively, 5%, 9%, 8%, and 3% lower, though BDS-3 VDOP, PDOP, and TDOP are 0–5% larger than GPS and Galileo in some small parts of the area. While compared with GLONASS, BDS-3 shows significant better DOPs in the whole study area, with the average HDOP, VDOP, PDOP, and TDOP being, respectively, 16%, 21%, 20%, and 14% lower.

The regional scale coverage of BDS-3 GEO and IGSO satellites improves the satellite visibility and in turn the DOPs in the covered areas. For each kind of DOPs, the improving rate of the regional (the study area) average relative to the global average is calculated (Table 5). The average improving rate of the NDOP (9%) is larger than that of the EDOP (4%), and the average improving rate of VDOP (16%) is the highest rate among all kinds of DOPs.

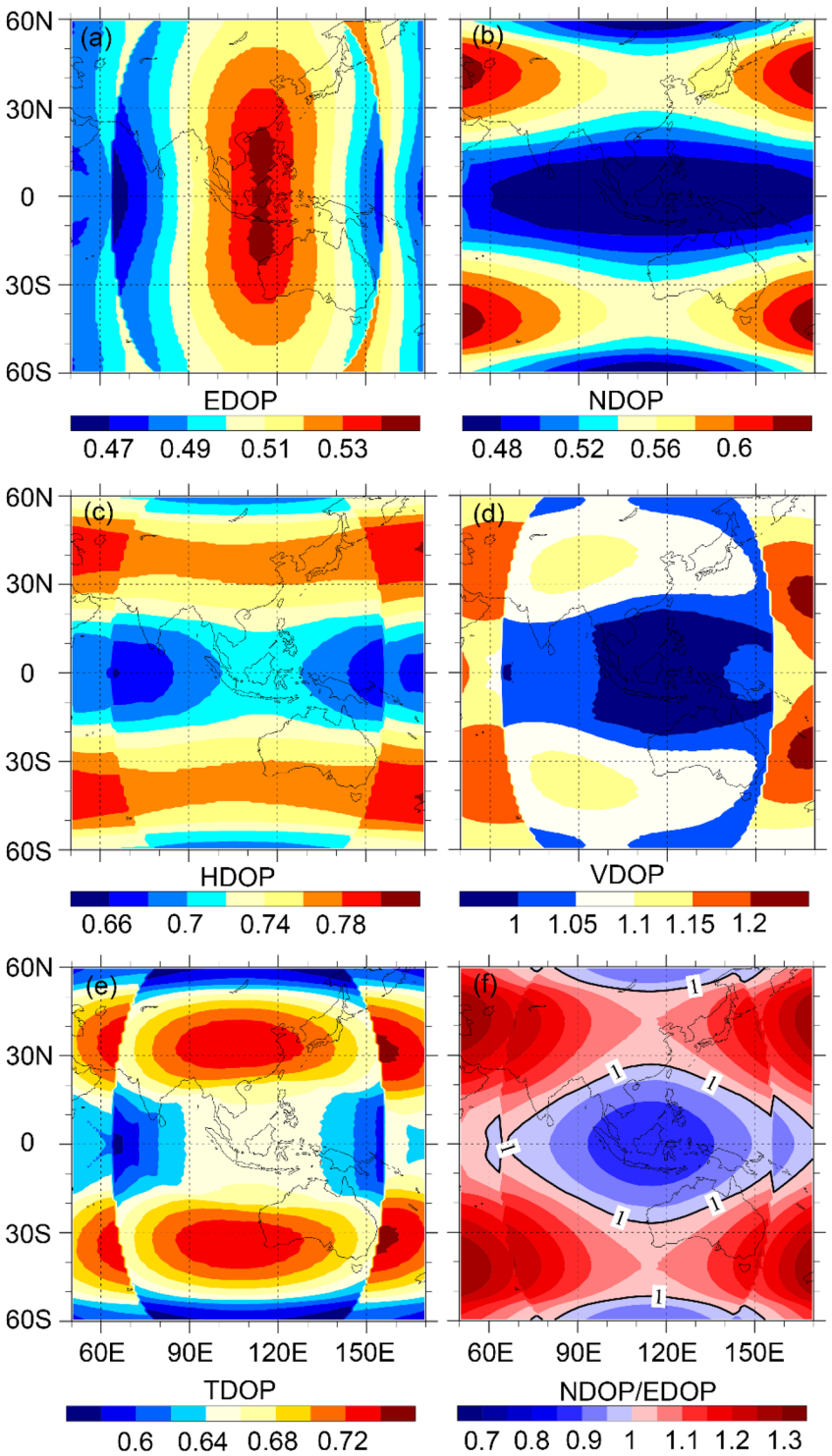

Fig. 11 Estimated DOPs of BDS-3 in the study area with a 5° CEA. **a** east DOP; **b** north DOP; **c** horizontal DOP; **d** vertical DOP; **e** time DOP; **f** NDOP-to-EDOP ratio. In **f**, the contours of the NDOP-to-EDOP ratios equal to 1 are marked

Conclusions

The BeiDou navigation satellite system with global coverage (BDS-3) is scheduled to be completed by 2020. Its performance and status among GNSSs are of great concern to global users. We modified the method of Wang et al. (2002) to assess GNSS performance in terms of satellite visibility and dilution of precision (DOP). While the original method is only for MEO constellations, the modified method is applicable to BDS-3 hybrid constellation. Also, the modified method is verified to give better estimations for MEO constellations. Validated by the reference values derived from real precise ephemerides, the accuracy of the estimated number of visible satellites is better than 0.15.

Table 3 DOP improving rates resulted from adding the 3 GEO, 3 IGSO, and 3GEO + 3IGSO satellites to M-BDS-3 in the study area

Constellation	DOP improving rate (%) Ave. (Min.~Max.)			
	HDOP	VDOP	PDOP	TDOP
3G + 24M	10 (5 ~ 17)	11 (1 ~ 23)	11 (4 ~ 20)	8 (1 ~ 20)
3I + 24M	9 (6 ~ 14)	11 (4 ~ 18)	10 (6 ~ 15)	8 (5 ~ 14)
3G + 3I + 24M	16 (13 ~ 19)	19 (8 ~ 29)	18 (10 ~ 25)	14 (7 ~ 25)

The DOP improving rate is defined as $\frac{DOP_M - DOP_{MG(MI\ or\ MGI)}}{DOP_M} \times 100\%$. The "Ave.", "Min.", and "Max." represent the average, minimal, and maximal DOP improving rates, respectively

Table 4 The average, minimal, and maximal DOP reduction rates of BDS-3 relative to the other three GNSSs over the study area

System	Reduction rates of BDS-3 DOPs relative to other GNSSs (%) Ave. (Min.~Max.)			
	HDOP	VDOP	PDOP	TDOP
(GPS-BDS)/GPS	5 (1 ~ 9)	9 (−3 ~ 20)	8 (−1 ~ 16)	3 (−5 ~ 15)
(GLO-BDS)/GLO	16 (9 ~ 22)	21 (6 ~ 33)	20 (8 ~ 29)	14 (5 ~ 28)
(GAL-BDS)/GAL	5 (1 ~ 9)	9 (−4 ~ 20)	8 (−1 ~ 16)	3 (−5 ~ 16)

The DOP reduction rate is defined as $\frac{DOP_{GPS(GLO\ or\ GAL)} - DOP_{BDS\text{-}3}}{DOP_{GPS(GLO\ or\ GAL)}} \times 100\%$

Table 5 Global and regional (the study area) average DOPs of BDS-3 and the DOP improving rates of the regional average relative to the global average

	EDOP	NDOP	HDOP	VDOP	PDOP	TDOP	GDOP
Global ave.	0.53	0.58	0.79	1.29	1.51	0.73	1.67
Regional ave.	0.51	0.53	0.74	1.08	1.30	0.67	1.47
Imp. rate (%)	4	9	6	16	14	8	12

The improving rate is defined as (*Glo.-Reg.*)/*Glo.* × 100%</tb>

This method underestimates the DOPs by less than 10% on average, and the DOP estimates reflect well the variation of their references over the latitudes. Traditionally, the satellite visibility and DOP are calculated from real or simulated ephemerides, however, this method estimates these values only using a few constellation parameters.

For the 24-MEO-only BDS (M-BDS-3), the latitudinal distributions of satellite visibility and DOP estimates are similar to those of GPS and Galileo. They all have less visible satellites at middle latitudes than at other latitudes and have largest NDOP at around 40° latitude. At the pole, they have minimal HDOP but have maximal VDOP. With a larger orbit inclination, the latitudinal distributions of GLONASS satellite visibility and DOP are clearly different from those of M-BDS-3, GPS, and Galileo. Comparing the NDOP-to-EDOP ratio of M-BDS-3 and the other three GNSSs indicates that a MEO-constellation GNSS with a lower orbit inclination has larger ratios over all latitudes except for the pole, where all GNSSs have a ratio close to one.

For BDS-3, with a 5° CEA, about 8–14 satellites can be observed around the globe. Regional disparities of satellite visibility and DOP resulted from the hybrid constellation of BDS-3 are significant. In the study area of 60°S–60°N and 50°E–170°E, the average number of visible BDS-3 satellites is more than the global average by 2.7. The regional (study area) average DOPs are 4–16% lower than the global averages. In this area, the number of BDS-3 visible satellites is more than for the other three GNSSs (by 1–7), and the DOPs of BDS-3 are lower than those of the other GNSSs (by 3–21%). Generally, the BDS-3 EDOP decrease from central longitude to the west and east ends of the area, while the NDOP increases from the equator to the middle latitudes. The BDS-3 NDOP-to-EDOP ratios show that, in the center of the area, including Southeast Asia and Northwestern Australia, the north positioning accuracy is higher than its east counterpart.

The results and conclusions of this study will enrich the growing knowledge base of the new-generation BDS. In addition, as an alternative way to calculate satellite visibility and DOP, the proposed method is not limited to the analysis of the existing GNSSs. It can also be used to analyze the geometry of other hybrid constellations, such as LEO-enhanced GNSS constellations, and can provide a basis for constellation selection and design.

Acknowledgements This study is supported by National Natural Science Foundation of China (41604017 and 41674029). We would like to express our gratitude to editor Alfred Leick and anonymous reviewers for their constructive comments and suggestions. We thank MGEX and GFZ for providing multi-GNSS orbit products.

Appendix 1: retrieval of 0.5° × 0.5° grid cells along the figure-8-shape track of BDS-3 IGSO satellites

We define a η-ξ coordinate system on the circular orbit plane of a BDS-3 IGSO satellite, with the η-axis pointing to the ascending node and the ξ-axis pointing to the satellite on the argument of latitude of 90°. The satellite positions on the circular orbit with an interval of 0.25° are

$$\begin{cases} \eta_i = R\cos\left(\frac{2\pi}{1440}i\right) \\ \xi_i = R\sin\left(\frac{2\pi}{1440}i\right) \end{cases} (i = 1, 2, ..., 1440) \tag{20}$$

where R is the distance between the satellite and the earth center (42,157 km). Their corresponding ECEF Cartesian coordinates are

$$\begin{pmatrix} X_i \\ Y_i \\ Z_i \end{pmatrix} = R_3(-\Omega_i)R_1(-i_{\text{orb}})\begin{pmatrix} \eta_i \\ \xi_i \\ 0 \end{pmatrix} (i = 1, 2, ..., 1440) \tag{21}$$

where $R_3(-\Omega_i)$ and $R_1(-i_{\text{orb}})$ are rotation matrices

$$R_3(-\Omega_i) = \begin{pmatrix} \cos\Omega_i & -\sin\Omega_i & 0 \\ \sin\Omega_i & \cos\Omega_i & 0 \\ 0 & 0 & 1 \end{pmatrix} \tag{22}$$

$$R_1(-i_{\text{orb}}) = \begin{pmatrix} 1 & 0 & 0 \\ 0 & \cos i_{\text{orb}} & -\sin i_{\text{orb}} \\ 0 & \sin i_{\text{orb}} & \cos i_{\text{orb}} \end{pmatrix} \tag{23}$$

where i_{orb} is the orbit inclination (55°) and Ω_i is the right ascension of ascending node. Let the satellite be right above the intersection point of subsatellite track (0°, 118°E) at time $t_0 = 0$, and the 1440 satellite positions be corresponding to the positions at time $t_i = i\Delta t$ $(i = 1, 2, ..., 1440)$, where$\Delta t = T/1440$ with $T = 86164$s (orbit period). Then the Ω_i can be written as

$$\Omega_i = 118°\frac{\pi}{180°} - \omega(t_i - t_0) = (118° - i \cdot 0.25°)\frac{\pi}{180°} \tag{24}$$

where ω is the angular velocity of the satellite.

From the Cartesian coordinates (X_i, Y_i, Z_i), the geocentric latitudeφ_i and longitude λ_i of the satellite can calculated as

$$\begin{cases} \varphi_i = \arcsin(\frac{Z_i}{R}) \\ \lambda_i = \arctan(\frac{Y_i}{X_i}) \end{cases} \tag{25}$$

We divide the spherical orbit surface (with the radius of R) into 0.5°×0.5° grid cells by geocentric latitude and longitude and use the satellite positions (φ_i, λ_i) $(i = 1, 2, ..., 1440)$ to determine which grid cells are on the figure-8-shape satellite track. The sampling interval of 0.25° for calculating the satellite positions ensures that all the 0.5° × 0.5° grid cells on the track are retrieved.

References

Bian S, Jin J, Fang Z (2005) The Beidou satellite positioning system and its positioning accuracy. Navigation 52(3):123–129

Cai C, He C, Santerre R, Pan L, Cui X, Zhu J (2016) A comparative analysis of measurement noise and multipath for four constellations: GPS, BeiDou, GLONASS and Galileo. Surv Rev 48(349):287–295

Cao Y, Hu X, Wu B, Zhou S, Liu L, Su R, Chang Z, He F, Zhou J (2012) The wide-area difference system for the regional satellite navigation system of COMPASS. Sci China Phys Mech 55(7):1307–1315

Chen J (2007) On precise orbit determination of low earth orbiters. Dissertation, Tongji University

Chen J, Chen Q, Wang B, Yang S, Zhang Y, Wang J (2017a) Analysis of inner-consistency of BDS broadcast ephemeris parameters and their performance improvement. In Proceedings of the ION Pacific PNT 2017 Conference, Honolulu, Hawaii, May 1–4, 2017

Chen J, Yang S, Zhou J, Cao Y, Zhang Y, Gong X, Wang J (2017b) A pseudo-range and phase combined SBAS differential correction model. Acta Geodaetica Cartogr Sin 46(5):537–546

Chiang K, Huang Y, Tsai M, Chen K (2010) The perspective from Asia concerning the impact of Compass/Beidou-2 on future GNSS. Surv Rev 42(315):3–19

CSNO (2012) Report on the development of BeiDou navigation satellite system (Version 2.1). China Satellite Navigation Office, Beijing

CSNO (2019) BeiDou navigation satellite system signal in space interface control document—open service signal B1I (Version 3.0). China Satellite Navigation office, Beijing

Eissfeller B, Ameres G, Kropp V, Sanroma D (2007) Performance of GPS, GLONASS and Galileo. In: Fritsch D (ed) Photogrammetric Week 07, Stuttgart, Germany, 3–7 September. 2007, Wichmann, Berlin Offenbach, pp 185–199

Gumilar I, Bramanto B, Kuntjoro W, Abidin H, Trihantoro N (2018) Contribution of BeiDou satellite system for long baseline GNSS measurement in Indonesia. In IOP Conference Series: Earth and Environmental Science 149(1):012070

Hauschild A, Montenbruck O, Sleewaegen J, Huisman L, Teunissen P (2012) Characterization of compass M-1 signals. GPS Solut 16(1):117–126

Hofmann-Wellenhof B, Lichtenegger H, Wasle E (2007) GNSS–global navigation satellite systems: GPS, GLONASS, Galileo, and more. Springer, Berlin

Kihara M, Okada T (1984) A satellite selection method and accuracy for the global positioning system. Navigation 31(1):8–20

Lou Y, Li X, Zheng F, Liu Y, Guo H (2018) Assessment and impact on BDS positioning performance analysis of recent BDS IGSO-6 satellite. J Navig 71(3):729–748
Meng X, Roberts G, Dodson A, Cosser E, Barnes J, Rizos C (2004) Impact of GPS satellite and pseudolite geometry on structural deformation monitoring: analytical and empirical studies. J Geod 77(12):809–822
Montenbruck O, Steigenberger P (2013) The BeiDou navigation message. J Glob Position Syst 12(1):1–12
Montenbruck O, Hauschild A, Steigenberger P, Hugentobler U, Teunissen P, Nakamura S (2013) Initial assessment of the COMPASS/BeiDou-2 regional navigation satellite system. GPS Solut 17(2):211–222
Parkinson B (1996) GPS error analysis. In: Parkinson B, Enge P, Axelrad P, Spilker J (eds) Global positioning system: theory and applications, vol I. American Institute of Aeronautics and Astronautics, Inc., Cambridge, Massachusetts, pp 469–484
Spilker J (1996) Satellite constellation and geometric dilution of precision. In: Parkinson B, Enge P, Axelrad P, Spilker J (eds) Global positioning system: theory and applications, Volume I. American Institute of Aeronautics and Astronautics, Inc., Cambridge, Massachusetts, pp 177–208
Wang J, Iz H, Lu C (2002) Dependency of GPS positioning precision on station location. GPS Solut 6(1–2):91–95
Wang G, de Jong K, Zhao Q, Hu Z, Guo J (2015) Multipath analysis of code measurements for BeiDou geostationary satellites. GPS Solut 19(1):129–139
Wanninger L, Beer S (2015) BeiDou satellite-induced code pseudorange variations: diagnosis and therapy. GPS Solut 19(4):639–648
Xiao W, Liu W, Sun G (2016) Modernization milestone: BeiDou M2-S initial signal analysis. GPS Solut 20(1):125–133
Yahya M, Kamarudin M (2008) Analysis of GPS visibility and satellite-receiver geometry over different latitudinal regions. In International Symposium on Geoinformation (ISG 2008): Kuala Lumpur, Malaysia, pp 13–15
Yang Y (2010) Progress, contribution and challenges of Compass/Beidou satellite navigation system. Acta Geodaetica Cartogr Sin 39(1):1–6
Yang Y, Xu J (2016) Navigation performance of BeiDou in polar area. Geomat Inf Sci Wuhan Univ 41(1):15–20
Yang Y, Li J, Xu J, Tang J, Guo H, He H (2011) Contribution of the compass satellite navigation system to global PNT users. Chinese Sci Bull 56(26):2813–2819
Yang Y, Li J, Wang A, Xu J, He H, Guo H, Shen J, Dai X (2014) Preliminary assessment of the navigation and positioning performance of BeiDou regional navigation satellite system. Sci China Earth Sci 57(1):144–152
Yang Y, Tang J, Montenbruck O (2017) Chinese navigation satellite systems. In: Teunissen P, Montenbruck O (eds) Springer handbook of global navigation satellite systems. Springer International Publishing, Cham, pp 273–304
Zhang Y, Chen J, Zhou J, Yang S, Wang B, Chen Q, Gong X (2016) Analysis and application of BDS broadcast ephemeris bias. Acta Geodaetica Cartogr Sin 45(S2):64–71
Zhang X, Wu M, Liu W, Li X, Yu S, Lu C, Wickert J (2017) Initial assessment of the COMPASS/BeiDou-3: New-generation navigation signals. J Geod 91(10):1225–1240
Zhang R, Tu R, Liu J, Hong J, Fan L, Zhang P, Lu X (2018) Impact of BDS-3 experimental satellites to BDS-2: service area, precise products, precise positioning. Adv Space Res 62(4):829–844

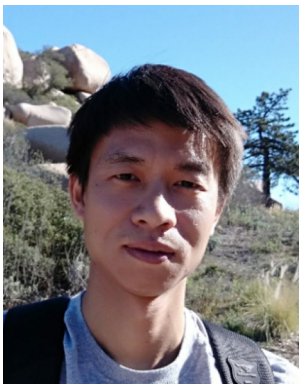

Minghua Wang Minghua Wang received the M.S. degree in geodesy and surveying engineering from Wuhan University, Wuhan, China, in 2009. He is currently a Ph.D. candidate at Tongji University, Shanghai, China. His research interests include GNSS meteorology, multipath mitigation for high-precision GNSS applications, and the navigation and positioning of BeiDou Navigation Satellite System (BDS).

Jiexian Wang Jiexian Wang is currently a professor at Tongji University. He obtained his Ph.D. degree from Shanghai Astronomical Observatory (SHAO), Chinese Academy of Sciences and have been working at Tongji University for 32 years. His main research interest is in the study of GNSS positioning and its applications.

Danan Dong Danan Dong is currently a professor at East China Normal University. He obtained his Ph.D. degree from Massachusetts Institute of Technology (MIT) and had worked in Jet Propulsion Laboratory (JPL) for 18 years. His main research interest is in the study of GNSS positioning and geophysics with application of GPS technology.

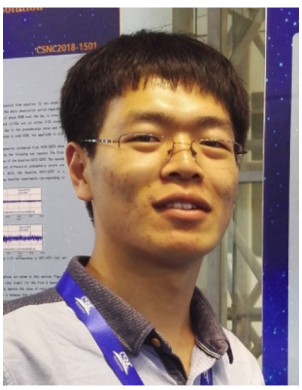

Lingdong Meng Lingdong Meng is currently a Ph.D candidate at the College of Surveying and Geo-Informatics, Tongji University, China. He received his B.S. degree from Liao Ning Technological University in 2016. His current research areas include multi-frequency GNSS data processing and the Low Earth Orbit (LEO) satellite constellation enhanced GNSS navigation and positioning.

Junping Chen Prof. Junping Chen is the head of the GNSS data analysis group at Shanghai Astronomical Observatory (SHAO). He received his Ph.D. degree in Satellite Geodesy from Tongji University in 2007. Since 2011, he has been supported by the "one hundred talents" program of Chinese Academy of Sciences. His research interests include multi-GNSS data analysis and GNSS augmentation systems.

Ahao Wang Ahao Wang is currently a Ph.D. candidate at the College of Surveying and Geo-Informatics, Tongji University, China. He has completed his B.S. at the School of Environment Science and Spatial Informatics in China University of Mining and Technology in 2015. His area of research focuses on the Multi-GNSS PPP and its application in geoscience.

Haomeng Cui Haomeng Cui is currently a M.S. candidate at the College of Surveying and Geo-Informatics, Tongji University, China. He has completed his B.S. at the School of Earth Sciences and Engineering, Hohai University, in 2017. His main research interest is in the navigation and positioning of BeiDou Navigation Satellite System (BDS).